Sensors and Materials, Vol. 38, No. 7 (2026) 3759–3784
MYU Tokyo

S & M 4534

Surface Albedo in Different Land Cover Types in Northeast China

Tao Pan,[1] Fu Li,[1*] Yucheng Tao,[1] Lijuan Zhang,[2] and Xiaoyan Jiang[1]

[1]Faculty of Science, Jiamusi University, Jiamusi 154007, China
[2]Heilongjiang Province Key Laboratory of Geographical Environment Monitoring and Spatial Information Service in Cold Regions, Harbin Normal University, Harbin 150025, China

(Received October 31, 2024; accepted September 29, 2025)

Keywords: surface albedo, land cover, MODIS, Northeast China

In this study, we use surface data (MCD43A3), snow cover data (MOD10A2) provided by the Moderate Resolution Imaging Spectroradiometer, and land cover products of the European Space Agency to analyze the spatiotemporal variation characteristics of surface albedo in Northeast China from 2001 to 2020. We quantified the differences in surface albedo between different land cover types under snow and nonsnow conditions. We found that the annual average surface albedo in Northeast China from 2001 to 2020 was about 0.21. The surface albedo has hardly changed over the past 20 years, but there are significant seasonal characteristics. The highest is in winter (0.36), followed by spring (0.18) and autumn (0.17), and the lowest is in summer (0.13). The overall spatial distribution characteristics are high in the east and west and low in the north, south, and central parts. The magnitude of albedo is related to different land cover types, mainly reflecting the significant difference in albedo between sparse low-vegetation and dense high-vegetation areas. When dense and high vegetation transitions to sparse and low vegetation, the albedo significantly increases, especially in winter when snow is present. These results would be beneficial for better understanding the land cover and eco-environment changes in Northeast China.

1. Introduction

Surface albedo refers to the ratio of solar radiation reflected by the Earth's surface to the incident solar radiation, reflecting the surface's reflective capacity to solar radiation. It determines the amount of radiation energy absorbed by the underlying surface and is one of the most important parameters in land surface process and climate models.(1) Surface albedo has been recognized as an important climate variable and a significant driving factor of climate change.(2) It affects the Earth's radiation balance by controlling the absorption and reflection of solar shortwave radiation at the surface. Subtle changes in surface albedo can significantly affect the radiation energy budget of the land-atmosphere system, thereby affecting local, regional, and global climate change.

*Corresponding author: e-mail: lifu@jmsu.edu.cn
https://doi.org/10.18494/SAM5443

ISSN 0914-4935
https://myukk.org/

Since Charney pointed out that an increase in surface albedo in desert regions can lead to regional climate aridification,[3] the climatic effects of surface albedo have gradually become a hot topic in Earth system science. Many scholars have conducted related research around this issue in recent years, finding that a decrease in surface albedo caused by snowmelt or vegetation greening leads to more solar radiation heating the surface and increasing surface temperature. Conversely, an increase in surface albedo affects atmospheric circulation, such as the tropical convergence zone and monsoons, leading to significant changes in precipitation and exacerbating the trend of aridification in arid regions.[4] Chen studied the distribution of and variation in surface albedo in China on the basis of statistical data from 16 solar radiation measurement stations in different regions.[5] He believes that the spatiotemporal variation in albedo is closely related to the natural surface characteristics and seasonal cycles of different regions. Liu *et al.*[6] and Zhang *et al.*[7] both demonstrated through field observations that surface albedo in vegetated areas exhibits significant interannual variations. However, owing to the limitations of observational data, there are significant errors in the calculation accuracy over large areas, making it difficult to further analyze the interannual amplitude and the relationship between the amplitude and other factors. With the continuous maturation of satellite remote sensing inversion methods, obtaining surface albedo over large areas, even globally, through satellite remote sensing data is considered to have a high degree of credibility.[8,9] The Moderate Resolution Imaging Spectroradiometer (MODIS) is a key sensor aboard the Terra and Aqua satellites that, with 36 spectral bands and 12-bit radiometric resolution, has the highest number of spectral bands of any global coverage moderate resolution imager. Numerous studies have verified that the MODIS-derived albedo product (MCD43A3) exhibits high overall accuracy and significant application value in global change research. Zhang[10] used MODIS surface albedo products (MCD43C3) to analyze the changes in surface albedo in the Xilingol grassland and its relationship with temperature and precipitation, finding that temperature is significantly correlated with surface albedo only at the beginning and end of the growing season, while precipitation is significantly negatively correlated with surface albedo throughout the growing season. Xu *et al.*[11] used MODIS surface albedo products (MCD43A3) to analyze the spatial distribution and variation characteristics of surface albedo in China from 2003 to 2017, finding that surface albedo changes more markedly in the Tianshan and northern regions and the northeast. Atlaskina *et al.*[12] combined MODIS surface albedo products with snow cover, temperature, vegetation index, and precipitation data to analyze the trend of surface albedo changes north of 50°N, suggesting that snow cover has a significant impact on regional surface albedo. Pang *et al.*[13] used CLARA-A2 surface albedo data from 1982 to 2015 to preliminarily analyze the spatiotemporal changes and determining factors of surface albedo in the Tibetan Plateau, suggesting that spatially, there is a negative correlation between albedo and vegetation.

The Northeast China region spans from the mid-temperate zone to the cold temperate zone from south to north. The temperature has increased by 1.43 °C in Northeast China over the past century, far greater than the global and national warming rates,[14,15] making it a sensitive area to climate warming and an ecologically fragile region. Additionally, owing to the diverse land cover types from south to north in Northeast China, including forests, shrubs, grasslands,

swamps, and croplands, it has a significant impact on the global ecological environment. The unique underlying surface and complex terrain of the Northeast China region have a significant impact on the changes in surface albedo. The albedo values of different underlying surface properties may vary considerably. Therefore, analyzing surface albedo on different land cover types within the regional spatial range is beneficial for understanding the dependence and sensitivity of surface parameters on land cover types in a macro perspective. In this study, we used a longer period of MODIS observation data (2001–2020) to reveal the seasonal and spatiotemporal variation characteristics of surface albedo in Northeast China. Furthermore, on the basis of the long-time series of Climate Change Initiative-Land Cover (CCI-LC) global land cover products, we analyzed the differences in surface albedo under different land cover types and studied the determining factors (underlying surface properties) related to albedo at spatial and temporal scales to elucidate the driving factors of surface albedo changes.

2. Overview of Study Area

The Northeast China region mainly consists of the three provinces of Heilongjiang, Jilin, and Liaoning, located in the mid- to high-latitude areas of the Northern Hemisphere, and is also the region with the highest latitude in China. It is bordered by the Heilongjiang River to the north with Russia, adjoins the Inner Mongolia Autonomous Region to the west, is adjacent to Russia and North Korea to the east, faces the Yellow Sea and the Bohai Sea to the south, with the Liaodong Peninsula obliquely inserted in between, and is adjacent to Hebei Province to the southwest. It extends from 118°53’E in the west to 135°05’E in the east, and from 38°43’N in the south to 53°33’N in the north. It spans nearly 17 longitudes from east to west and 15 dimensions from north to south (Fig. 1). The total area of the region is approximately 78.94×10^4 km^2 (it does not include the Gagdaqi and Songling regions of the Inner Mongolia Autonomous Region led by Heilongjiang Province and the surrounding islands of Liaoning Province). The region has a distinct continental monsoon climate, generally characterized by a cold temperate to warm temperate continental monsoon climate. It spans from the warm temperate zone in the south to the mid-temperate and cold temperate zones in the north, with a clear north–south temperature gradient. The annual average temperature in the northwest and northeast is less than 3 °C, while the central plain has an annual average temperature between 3 and 7 °C. The northeast region has a cold climate, with an average January temperature below −4 °C and an average summer temperature above 24 °C. Precipitation decreases from the east to the central to the western parts, with annual cumulative precipitation amounts of 600–1000, 300–600, and 100–300 mm, respectively. Additionally, the northeast region has a diverse and complex topography, mainly consisting of plains, mountains, and hills. The eastern part is the Changbai Mountain Range, the northern part is the Lesser Xing’an Range, the western part leans on the Greater Xing’an Range, and the east, north, and west are surrounded by low- and medium-height mountains. The central part is a vast plain, which consists of, from south to north, the Liaohe, Songnen, and Sanjiang Plains. Together, they form one of China’s largest plains, the Northeast Plain.

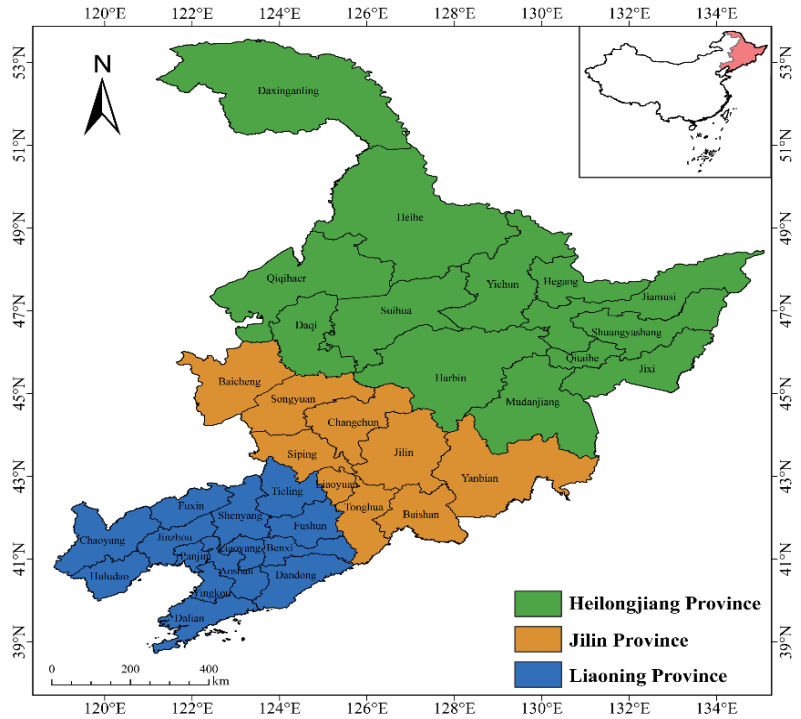

Fig. 1. (Color online) Location and administrative divisions of Northeast China.

3. Data and Methods

3.1 Datasets

The surface albedo data used in this study were derived from the MODIS BRDF/Albedo product series - MCD43A3 dataset (https://lpdaac.usgs.gov/products/mcd43a3v061/). This product employs a method of cumulative observation weighting, using the data from the 9th day of every 16-day cycle as a reference. It produces the daily albedo product by weighting the observational data from the preceding 8 days and the following 8 days, thereby enhancing the temporal resolution to 1 day with a spatial resolution of 500 m. The MCD43A3 dataset has been extensively validated against ground observation data and is considered to have a high degree of accuracy.[16,17] The MCD43A3 dataset includes black-sky albedo and white-sky albedo for seven narrow bands and three broad bands (visible light band 0.3–0.7 μm, near-infrared band 0.7–5.0 μm, and shortwave band 0.3–5.0 μm), as well as data quality flags. Black-sky albedo and white-sky albedo represent the albedo under fully direct and fully diffuse solar radiation conditions, respectively, which correspond to conditions of completely clear and completely overcast skies. In this study, we focused on the black-sky albedo at noon (local time) in the shortwave band because this band reflects the surface's albedo to direct sunlight at noon and reduces the uncertainty of the results.[10] Additionally, we only selected grid data with data quality flags of 0

(best quality) or 1 (good quality) for analysis. The data are processed through the Google Earth Engine platform and are mosaicked, clipped, and operated using the vector boundary of the northeast region.

The snow cover data was obtained from the MOD10A2 dataset provided by the MODIS sensor on the Terra satellite (https://nsidc.org/data/mod10a2/versions/61). It is an 8-day synthesized snow cover product reflecting the maximum snow cover extent during this period, with a resolution of 500 m. MOD10A2 can effectively reduce cloud interference and meet the requirements of long-term and high-precision snow research.[18] In this study, we utilized it to extract the snow cover area in Northeast China in winter.

Land cover data are sourced from the CCI-LC global land cover product developed by the European Space Agency. This dataset is not only highly accurate but also has the longest time series (1992–2020) and has a relatively high spatial resolution (300 m) among global land cover products.[19,20] It is highly suitable for large-scale, long-term series studies of land cover changes. The data format is TIFF, with the coordinate system being WGS1984. The data can be obtained through the following website (http://maps.elie.ucl.ac.be/CCI/viewer/index.php). The CCI-LC dataset has a fine classification of land cover types, and the product divides land use types into 22 major categories and 37 subcategories according to the land cover classification system developed by the Food and Agriculture Organization of the United Nations. To better maintain data consistency, we reclassified the land cover types according to a merging scheme (Table 1).

3.2 Methods

3.2.1 Trend analysis

Trend analysis on the time series of albedo was carried out by the linear trend estimation method.

$$y = ax + b \tag{1}$$

Here, a and b are constants, and x represents the year. The trend coefficient a and the regression coefficient b are obtained by least squares. The value of a being positive or negative represents the direction of the data series change with time, and the absolute value of a represents the rate of change.[21]

3.2.2 Variance analysis

One-way analysis of variance is used to study whether different levels of a control variable have a significant impact on the observed variables. The analysis of r groups, each containing k observations, is called a one-way analysis of variance with equal numbers of observations between groups.[21]

Table 1
Land cover types consolidation scheme of CCI-LC.

Rainfed cropland	10 cropland, rainfed; 11 herbaceous cover; 12 tree or shrub cover
Irrigated cropland	20 cropland, irrigated or post-flooding
Mosaic cropland	30 mosaic cropland (>50%) / natural vegetation (tree, shrub, herbaceous cover) (<50%)
Mosaic vegetation	40 mosaic natural vegetation (tree, shrub, herbaceous cover) (>50%) / cropland (<50%)
Evergreen broadleaved forest	50 tree cover, broadleaved, evergreen, closed to open (>15%)
Deciduous broadleaved forest	60 tree cover, broadleaved, deciduous, closed to open (>15%); 61 tree cover, broadleaved, deciduous, closed (>40%); 60 tree cover, broadleaved, deciduous, open (15–40%)
Evergreen needleleaved forest	70 tree cover, needleleaved, evergreen, closed to open (>15%); 71 tree cover, needleleaved, evergreen, closed (>40%); 72 tree cover, needleleaved, evergreen, open (15–40%)
Deciduous needleleaved forest	80 tree cover, needleleaved, deciduous, closed to open (>15%); 81 tree cover, needleleaved, deciduous, closed (>40%); 82 tree cover, needleleaved, deciduous, open (15–40%)
Mixed forest	90 tree cover, mixed leaf type (broadleaved and needleleaved); 100 mosaic tree and shrub (>50%) / herbaceous cover (<50%)
Mosaic herbaceous	110 mosaic herbaceous cover (>50%) / tree and shrub (<50%)
Shrubland	120 shrubland; 121 evergreen shrubland; 122 deciduous shrubland
Grassland	130 grassland; 140 lichens and mosses
Sparse vegetation	150 sparse vegetation (tree, shrub, herbaceous cover) (<15%); 151 sparse tree (<15%); 152 sparse shrub (<15%); 153 sparse herbaceous cover (<15%)
Swamp	160 tree cover, flooded, fresh or brackish water; 170 tree cover, flooded, saline water; 180 shrub or herbaceous cover, flooded, fresh/saline/brackish water
Urban areas	190 urban areas
Bare areas	200 bare areas; 201 consolidated bare areas; 202 unconsolidated bare areas
Water	210 water bodies
Ice	220 permanent snow and ice

In the calculation of one-way analysis of variance, the following equations are used:

$$SS_A = \sum_{i=1}^{r}\sum_{j=1}^{k}\left(\overline{X}_i - \overline{X}_{ij}\right)^2, \tag{2}$$

$$SS_E = \sum_{i=1}^{r}\sum_{j=1}^{k}\left(X_{ij} - \overline{X}_i\right)^2, \tag{3}$$

$$MS_A = \frac{1}{r-1}\sum_{i=1}^{r}\sum_{j=1}^{k}\left(\overline{X}_i - \overline{X}_{ij}\right)^2, \tag{4}$$

$$MS_E = \frac{1}{n-r}\sum_{i=1}^{r}\sum_{j=1}^{k}\left(X_{ij} - \overline{X}_i\right)^2. \tag{5}$$

The samples of each random variable are called a group, and $\overline{X}_i$ is the mean value of group i. The mean value of all X_{ij} is called the overall mean value. SS_A is the sum of the squares of the deviations between the mean values of each group and the overall mean value, i.e., the sum of the squares of the deviations between groups, reflecting the differences among groups. SS_E is the sum of the squares of the deviations in each group, reflecting the difference in each group. The degree of freedom of SS_A is $v_1 = r - 1$. The degree of freedom of SS_E is $v_2 = r(k - 1)$. MS_A is the mean-square deviation between groups, and MS_E is the mean-square deviation within groups.

3.2.3 Coefficient of variation

The coefficient of variation, also known as the "coefficient of dispersion," is a normalized measure of the degree of dispersion of a probability distribution and is defined as the ratio of the standard deviation to the mean value:

$$C_v = \frac{\sigma}{\mu}, \tag{6}$$

where σ is the standard deviation and μ is the mean value.[21]

3.2.4 Mann–Kendall test

The Mann–Kendall (M–K) test is a type of nonparametric statistical test method.[22] Its advantage is that it does not need the sample to follow a certain distribution, and it is not affected by a few outliers. It is more suitable for type and sequence variables, and the calculation is more convenient.

For time series X with n sample sizes, a rank series is constructed:

$$S_k = \sum_{i=1}^{k} r_i \qquad (k = 2,3,4,\ldots,n), \tag{7}$$

where

$$r_i = \begin{cases} 1 & x_i > x_j \\ 0 & \text{else} \end{cases} \qquad (j = 1,2\ldots,i). \tag{8}$$

S_k is a rank sequence composed of the cumulative count of values at time i that exceed those at subsequent time points.

Under the assumption of random independence of time series, a statistic is defined as

$$UF_k = \frac{\left[S_k - E\left(S_k\right)\right]}{\sqrt{Var\left(S_k\right)}} \qquad \left(k = 1,2,\ldots,n\right), \tag{9}$$

where $UF_i = 0$, $E(S_k)$ and $Var(S_k)$ are the mean and variance of S_k, respectively. When x_1, x_2, ..., x_n are independent of each other and have the same continuous distribution, they can be calculated using the following formulas:

$$E\left(S_k\right) = \frac{n\left(n+1\right)}{4}, \tag{10}$$

$$Var\left(S_k\right) = \frac{n\left(n-1\right)\left(2n+5\right)}{72}. \tag{11}$$

UF_i is the standard normal distribution. At a given significance level α, look up the normal distribution table. If $UF_i \mid > U_\alpha$, it indicates that there is a clear trend change in sequence. According to the time series X in reverse order (x_n, x_{n-1}, ..., x_1), the above process was repeated, and the variables $UB_k = -UF_k$, $k = n$, $n - 1$, ..., 1, $UB_k = 0$ were constructed.

The advantage of the M–K test is that it is not only simple to calculate, but can also determine the time of mutation initiation and point out the mutation region. Therefore, it is a common method to analyze mutation.

3.2.5 Pettitt test

We performed the Pettitt test as it has been proven to be one of the most convenient statistical methods for detecting abrupt changes in time series data.[23] The formula is given as

$$U_{t,n} = U_{t-1,n} + \sum_{i-1}^{n} \operatorname{sgn}\left(x_t - x_i\right), \quad t = 2,3,\ldots,n, \tag{12}$$

where x_t and x_i represent the tth and ith time series samples, respectively. If t meets the condition

$$K_t = \max_{1 \le t \le n} \left|U_{t,n}\right|, \tag{13}$$

then point t is the mutation point. We establish the test statistic p to verify the significance of the mutation point. The formula is given as

$$p = 2\exp\left[-6\left(K_t^2\right) / \left(n^3 + n^2\right)\right]. \tag{14}$$

If $p \leq 0.05$, the detected mutation point is deemed statistically significant; conversely, it is considered nonsignificant.

4. Results and Analysis

4.1 Temporal variation in surface albedo in Northeast China

The average annual surface albedo in Northeast China from 2001 to 2020 is approximately 0.21, with the highest value occurring in 2013, around 0.26, and the lowest value in 2019, around 0.17, a difference of 0.09. The coefficient of variation is 0.10, indicating that the interannual variation in surface albedo in Northeast China is close to 10%. It can be observed from the interannual changes (Fig. 2) that over the past 20 years, the rate of change in annual surface albedo in Northeast China has been about 0.001/10a ($P > 0.05$), which does not pass the significance test. The results of the M–K test show that the surface albedo in Northeast China has not changed significantly over the past 20 years. Multiple mutation points were detected within the 2004–2010 period in Northeast China's surface albedo data; however, the mutation test did not pass the significance level test, indicating that although there are mutations in the surface albedo changes in Northeast China, there is no significant mutation year.

Surface albedo, which typically depends on the solar zenith angle, varies considerably with the seasons. Therefore, analyzing the temporal variation in surface albedo in different seasons is of significant importance. From 2001 to 2020, the average surface albedo values in Northeast China for spring, summer, autumn, and winter were 0.18, 0.13, 0.17, and 0.36, respectively. It can be observed that the surface albedo is highest in winter, followed by spring and autumn, with the lowest surface albedo in summer, approximately one-third of that in winter. From the interannual

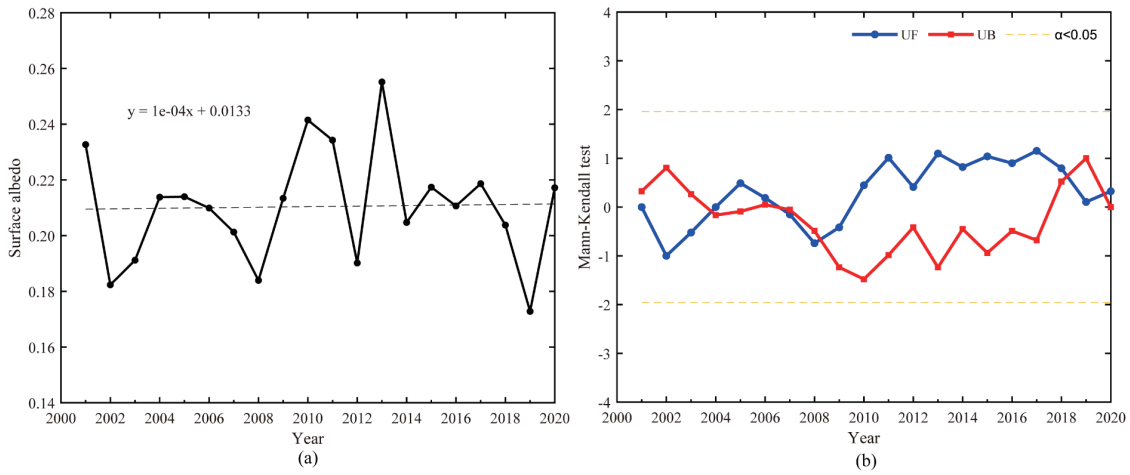

Fig. 2. (Color online) Interannual variation in surface albedo from 2001 to 2020 in Northeast China. (a) annual variation and (b) M–K test.

change trends for each season (Fig. 3) over the past 20 years, the rate of change in surface albedo for each season in Northeast China has been less than 0.001/10a ($P > 0.05$), and none have passed the significance test. Therefore, there has been almost no change in surface albedo on an interannual scale for spring, summer, autumn, and winter. The coefficients of variation in surface albedo in spring, summer, autumn, and winter are 0.13, 0.02, 0.08, and 0.15, respectively. The variation range of surface albedo in winter and spring is larger, about 15%, which is significantly higher than that in summer and autumn. It is mainly related to the degree of snow cover. The snow-covered underlying surface will significantly increase the value of surface albedo.

The results of the M–K test showed that the seasonal surface albedo changes in Northeast China have not been significant since 2001, but there are multiple mutation points in the surface albedo in spring, summer, and winter (Fig. 4). The main distribution is between 2004 and 2008 and 2016–2020, but the mutation test did not pass the significance level test. There is only one mutation point in autumn, but there is no significant change trend before and after the mutation point. Combining the results of the Pettitt test, we found that the mutation point does not pass the

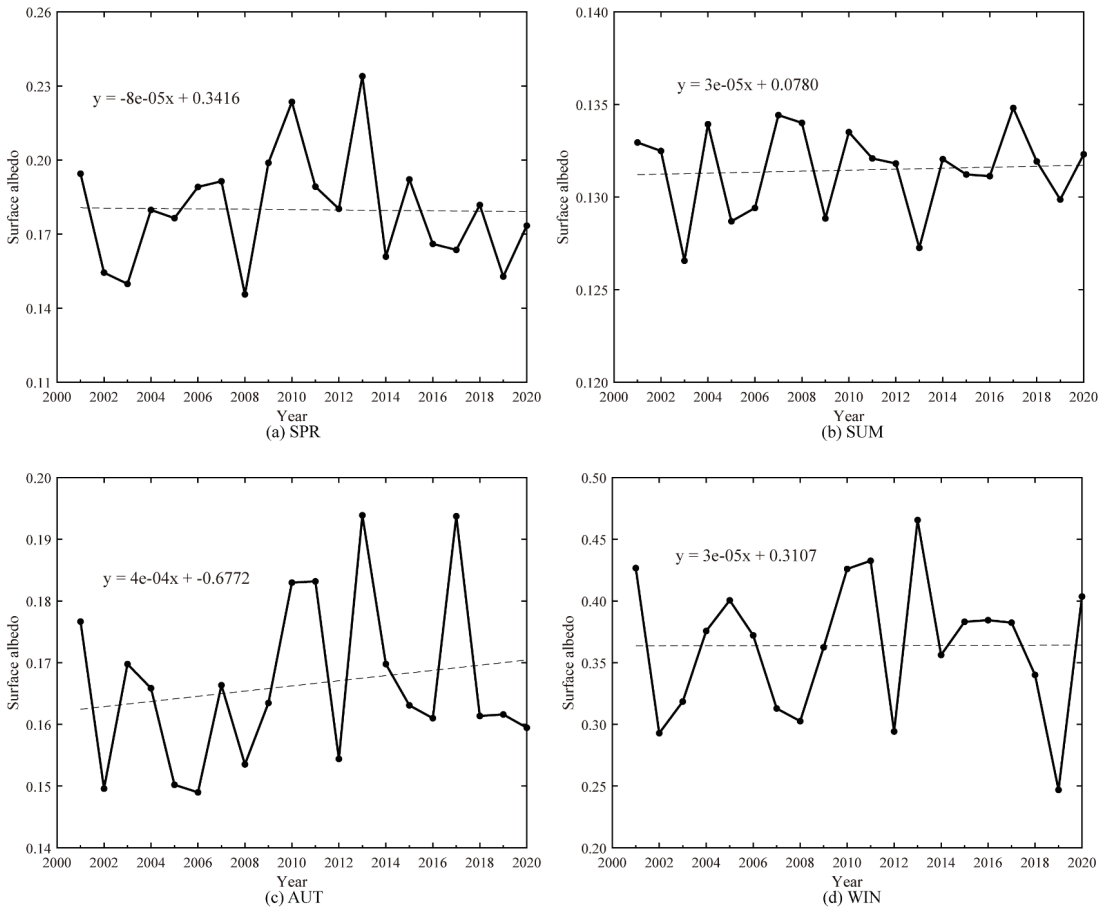

Fig. 3. Seasonal variation in surface albedo in Northeast China from 2001 to 2020. (a) SPR, (b) SUM, (C) AUT, and (d) WIN.

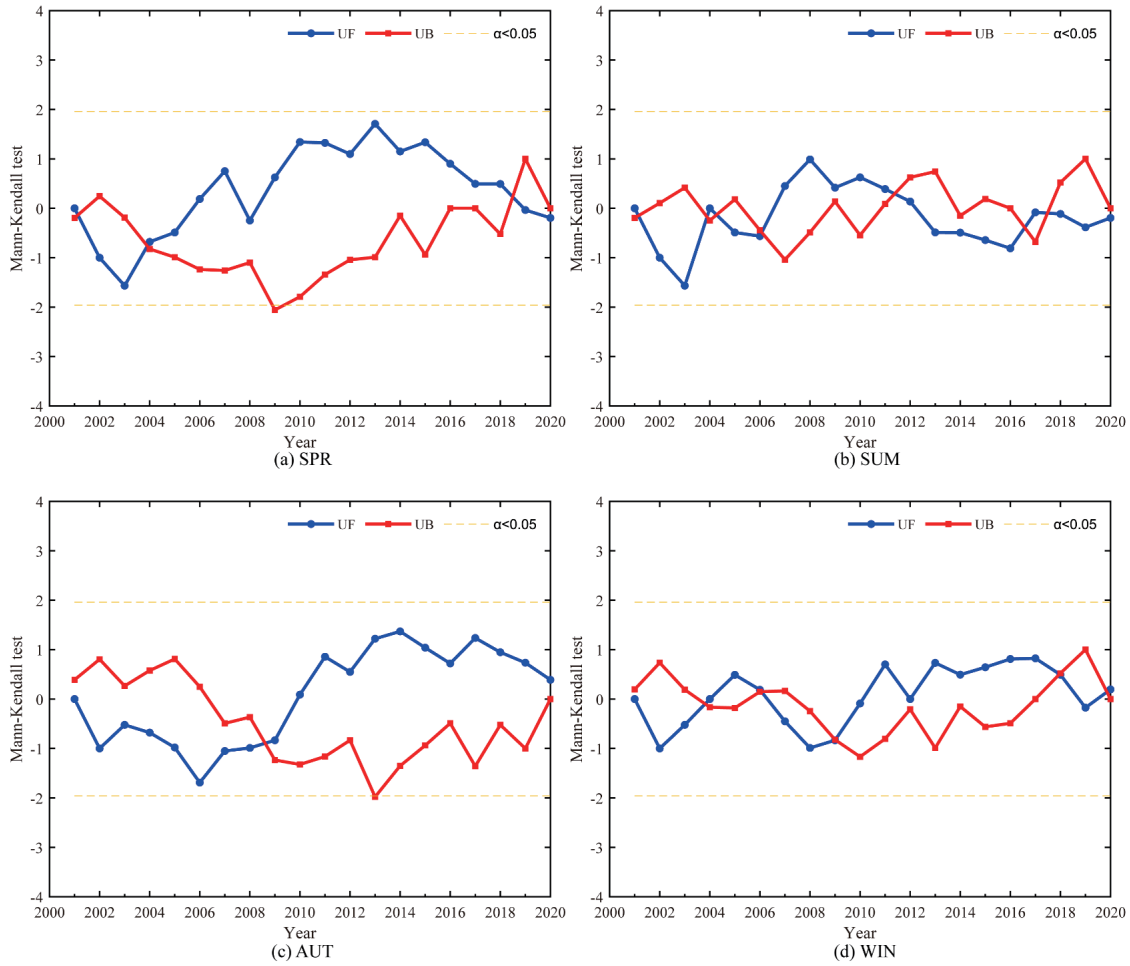

Fig. 4. (Color online) Results of the M–K test of surface albedo in different seasons in Northeast China from 2001 to 2020. (a) SPR, (b) SUM, (C) AUT, and (d) WIN.

significance test, indicating that although the surface albedo in different seasons shows a mutation, there is no significant mutation year.

In this study, we compared the differences in surface albedo among spring, summer, autumn, and winter seasons through analysis of variance. The results showed that there is a highly significant difference ($P < 0.01$) in surface albedo between winter and spring, summer, and autumn in Northeast China (Fig. 5), with winter surface albedo being significantly higher than in other seasons. There is also a highly significant difference ($P < 0.01$) in surface albedo between summer and spring, and summer and autumn, with summer surface albedo being significantly lower than in other seasons. However, there is no significant difference in surface albedo between spring and autumn. Therefore, it can be seen that the level of albedo is mainly related to the nature of the underlying surface, especially the presence or absence of snow cover. The study area is located in a mid to high-latitude region with distinct seasons and complex underlying surface characteristics. This area experiences snow accumulation in winter and lush

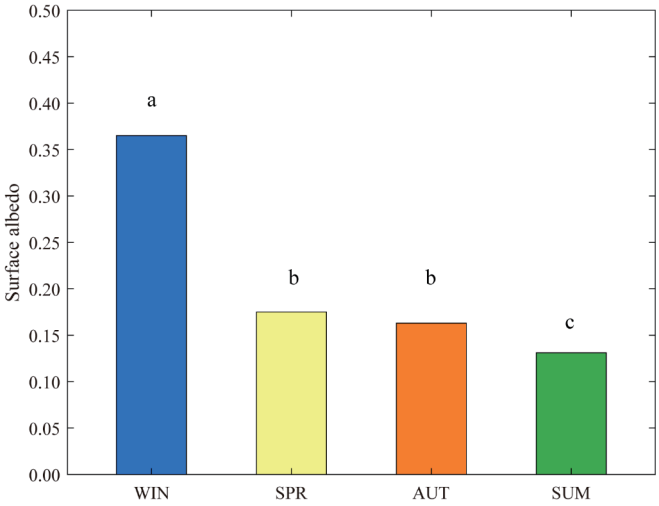

Fig. 5. (Color online) Bar chart of surface albedo and results of variance analysis in different seasons.

vegetation in summer. The spring and autumn seasons are the snowmelt and snow accumulation periods, respectively. Hence, the surface albedo in Northeast China shows a significant difference in comparison with other seasons during winter.

4.2 Spatial distribution characteristics of surface albedo

Figure 6 shows the spatial distribution of the annual average surface albedo in Northeast China from 2001 to 2020. It can be observed that over the past 20 years, the annual average surface albedo in Northeast China has exhibited strong spatial heterogeneity, with a general pattern of higher values in the east and west and lower values in the south, north, and central areas. Specifically, the reflectance is relatively high in the eastern, western, and northern parts of the study area, such as the Sanjiang Plain, Songnen Plain, and Heihe region, with the highest reflectance reaching 0.46. In contrast, the surface albedo is relatively lower in the southwestern and southeastern parts of the study area, such as Liaoning, Mudanjiang, Yanbian, and Baishan, as well as in the northern and northwestern parts, including Yichun and the Daxing'anling region, with albedo values ranging between 0.10 and 0.20. Overall, it shows that the surface albedo in the Songnen and Sanjiang Plains is significantly higher than that in the mountainous areas of the Greater and Lesser Xing'an Mountains.

Figure 7 shows the spatial distribution of surface albedo in different seasons in Northeast China from 2001 to 2020. It can be observed that over the past 20 years, the surface albedo in each season in Northeast China has shown significant spatial heterogeneity, particularly in winter. The albedo values are distributed across the range from 0.1 to 0.9, generally being higher in the east and west and lower in the south, north, and central areas. The high albedo values are mainly related to snow cover and the nature of the underlying surface, especially in agricultural fields and areas with low and sparse vegetation, such as the Sanjiang Plain, Songnen Plain, and

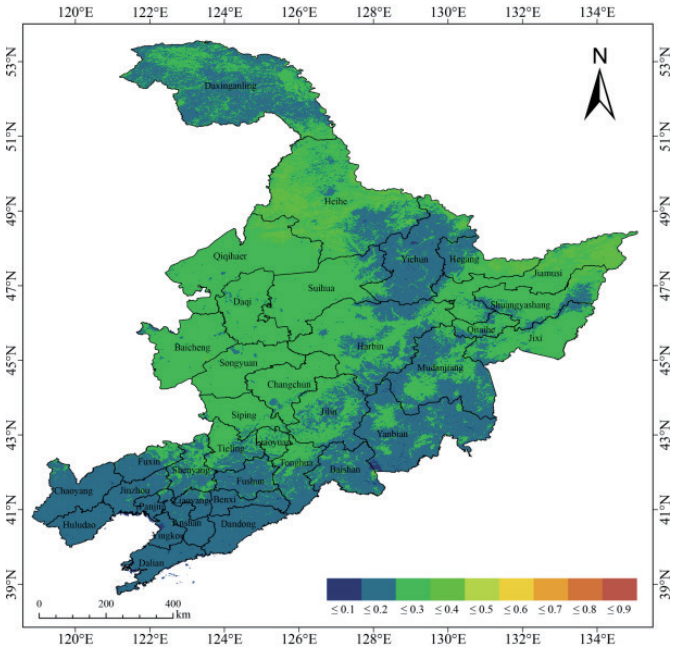

Fig. 6. (Color online) Spatial distribution of annual average surface albedo in Northeast China from 2001 to 2020.

Heihe region, where surface albedo is high, reaching above 0.5. In contrast, in the Greater and Lesser Xing'anling regions and the Mudanjiang area, where the vegetation is dense with forests, the albedo is relatively lower, generally below 0.5. Note that in Liaoning, owing to its southern latitude and lower snow cover, the albedo is also relatively low, with a minimum value of around 0.02. In spring, as the snow melts, the spatial heterogeneity of surface albedo gradually decreases. The Songnen Plain, Sanjiang Plain, and western side of the Daxing'anling region in northern Heilongjiang have a relatively high albedo, around 0.4. In Liaoning Province, eastern Jilin Province, southeastern Heilongjiang, and areas such as Yichun in central and northern Heilongjiang, the albedo is relatively lower, generally below 0.2. In summer, the surface albedo across the entire study area tends to be consistent, maintaining between 0.1 and 0.2, with only the Baicheng and Songyuan areas in western Jilin Province reaching an albedo of 0.3. In autumn, the albedo in the western Songnen Plain and the eastern Sanjiang Plain of Heilongjiang has increased to around 0.3, and the albedo in other areas generally remains below 0.2.

4.3 Spatial variation characteristics of surface albedo

The interannual spatial variation in surface albedo plays an indispensable role in assessing surface radiation balance, especially in a long timescale, where the interannual spatial variation in surface albedo can have a significant impact on regional climate. Therefore, in this study, we employed Eq. (1) to conduct a trend analysis on the surface albedo for the entire year and the four seasons—spring, summer, autumn, and winter—from 2001 to 2020. The aim is to reveal the

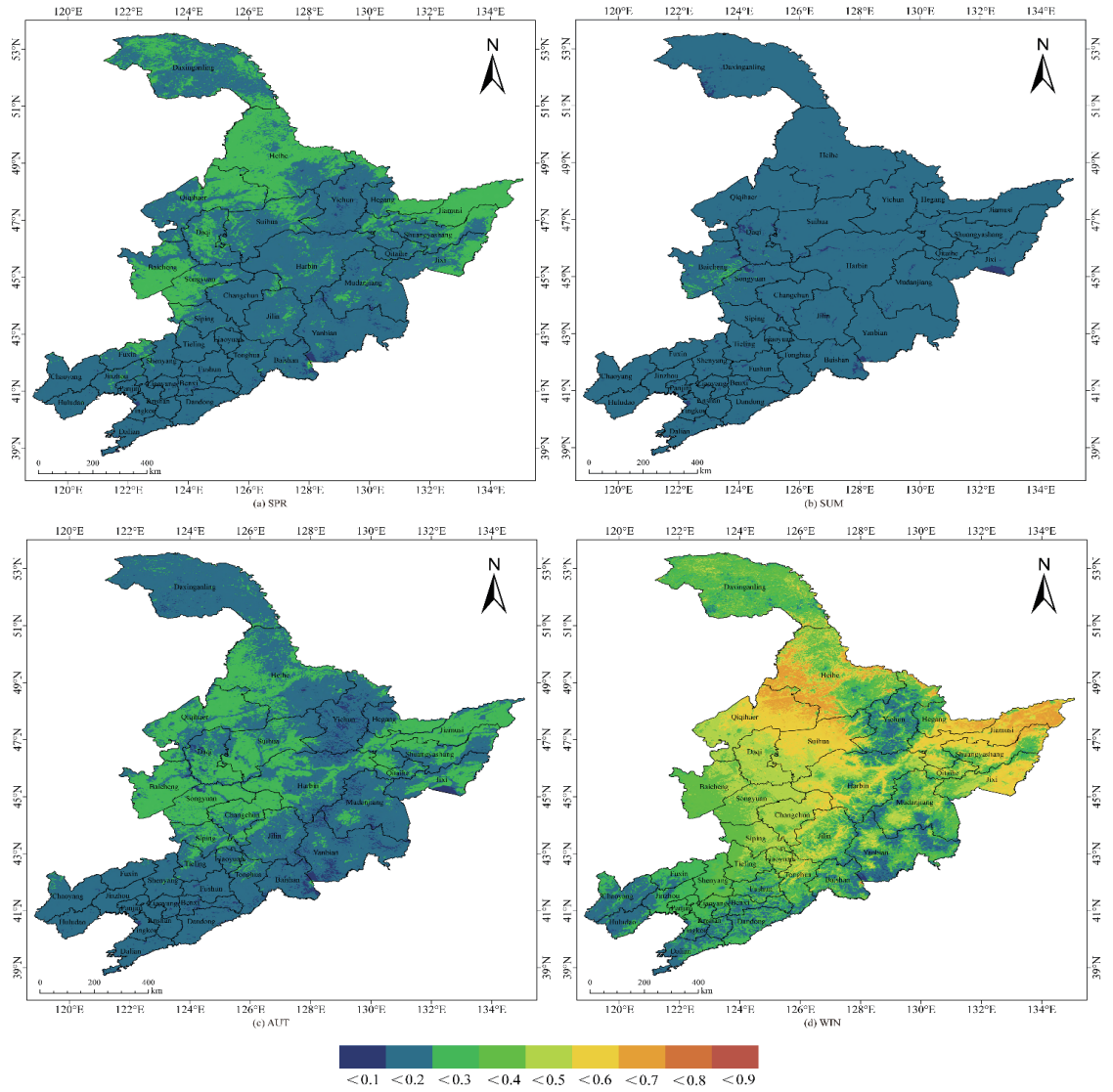

Fig. 7. (Color online) Spatial distribution of seasonal average surface albedo in Northeast China from 2001 to 2020.

characteristics and determining factors of the interannual changes in surface albedo over the past two decades.

In this study, a trend analysis was performed on the albedo values of each grid cell in the study area over the past 20 years. When slope a is positive, it indicates an increasing trend in reflectivity; when a is negative, it indicates a decreasing trend. To more accurately represent the spatial trend changes in albedo, we only select grid points that meet the significance test for analysis. Figure 8 shows the spatial trend of the annual average surface albedo.

Figure 8 indicates that from 2001 to 2020, the interannual change trend of surface albedo in most areas of the northeast region is not significant, with only 11.41% of the total area showing

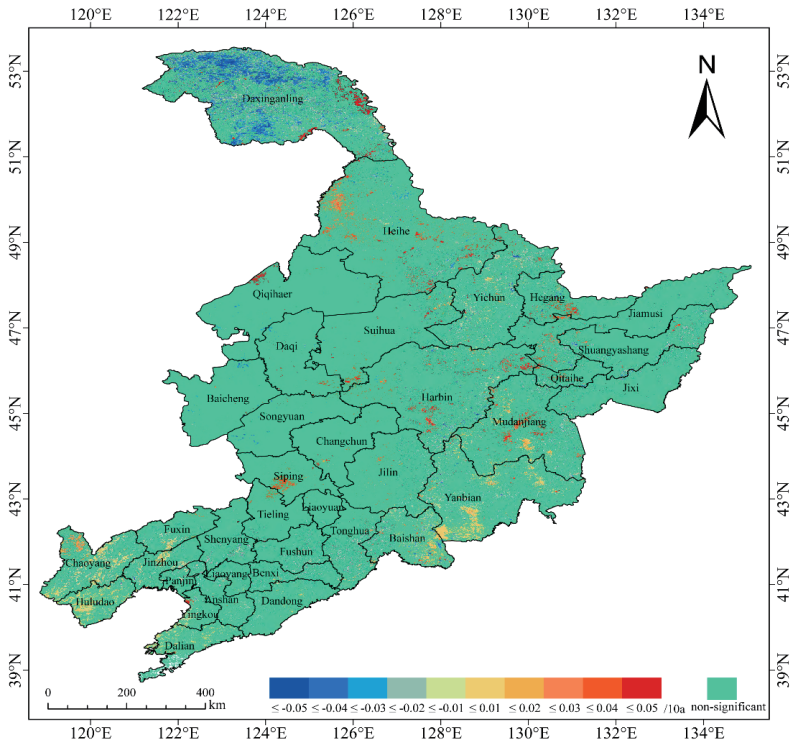

Fig. 8. (Color online) Spatial distribution of interannual variation in surface albedo in Northeast China from 2001 to 2020.

significant changes. Approximately 7.29% of the grid points exhibit a significant decreasing trend, with an average change rate of about −0.02/10a, mainly distributed in the northwestern Daxing'anling area of the study region. Grid points showing a significant increasing trend account for about 4.12% of total area and are concentrated in areas such as the northern part of Heilongjiang Province around Nenjiang, the southern part of Jilin Province around Siping, the eastern part around Baishan and Yanbian, and the southwestern part of Liaoning Province around Chaoyang and Huludao. In the southern, central, and northern parts of the study area, significant changes are only sporadically distributed. Notably, in areas such as the west of Qiqihar, the west of Huma, the south of Xinlin District, and the city of Mudanjiang, the increasing rate is relatively large, above 0.05/10a.

Figure 9 illustrates the spatial trend of surface albedo changes for spring, summer, autumn, and winter. It can be observed that both spring and winter surface albedo values are predominantly characterized by significant decreases, with the areas of significant decrease concentrated in the northwestern Daxing'anling region. In spring, the grid points showing a significant decrease account for approximately 6.50% of the total area, with a reduction rate of about −0.03/10a. The grid points showing a significant increase only account for 2.75% of total area, mainly concentrated in the west of Qiqihar, with an average change rate of about 0.02/10a. In winter, the grid points showing a significant decrease account for about 6.44% of the total area, distributed across the Greater and Lesser Xing'anling regions and the southern part of Liaoning Province, including Jinzhou, Panjin, Liaoyang, and Yingkou, reaching the highest

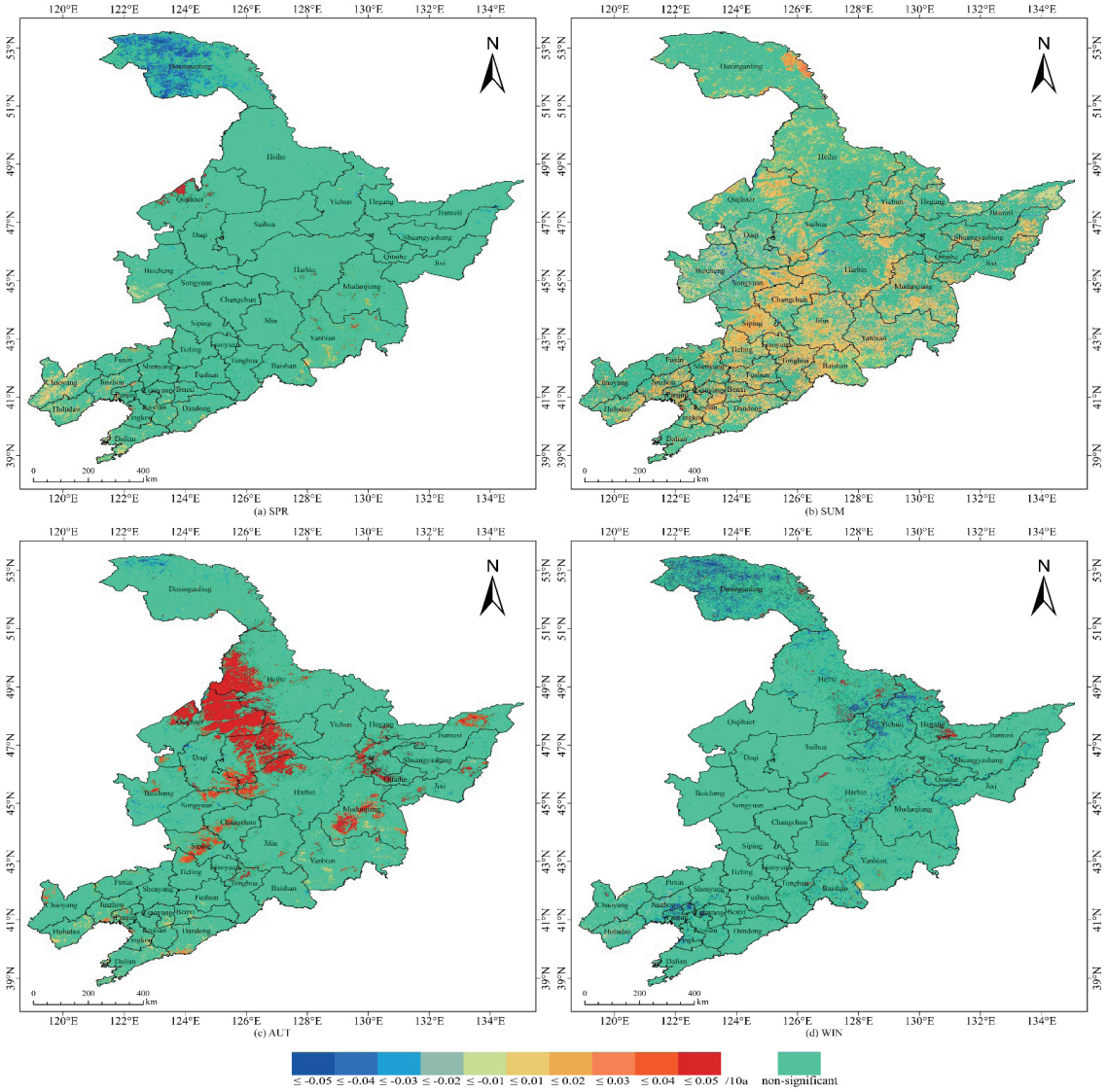

Fig. 9. (Color online) Spatial distribution of interannual seasonal variation in surface albedo in Northeast China from 2001 to 2020.

reduction rate of −0.04/10a. The grid points showing a significant increase in winter account for about 2.09% of the total area, with more concentrated distributions in the central part of Yanbian, Hegang, and in the southern part of Hegang, with an average change rate of about 0.07/10a.

The land surface albedo increased significantly in summer and autumn, and the area with the significant increase in summer accounted for about 39.98% of the total area of the whole region, and the change rate was about 0.01/10a on average, which was mainly distributed in most areas of Jilin and Liaoning provinces. In addition, it is also continuously distributed in the Songnen Plain, Sanjiang Plain, and northern Huma County of Heilongjiang Province. The areas of significant decrease in summer accounted for about 7.62% of the total area of the whole region,

mainly scattered in Baicheng, Daqing, Songyuan, and Harbin, and the average decrease rate was about −0.01/10a. The areas with significant increases in autumn were mainly distributed in the Songnen Plain. In addition, the Sanjiang Plain in eastern Heilongjiang Province and Mudanjiang, Ning 'an, and Muleng in southeast Heilongjiang Province also had a lamellate distribution, accounting for 14.97% of total area of Heilongjiang Province, and the increase rate was about 0.04/10a on average. In addition, some areas in the northern part of the Greater Hinggan Mountains showed a significant decrease trend. It accounted for about 1.68% of the total area, and the reduction rate was about −0.03/10a on average.

In general, the surface albedo in all seasons in the plain area is significantly higher than that in the mountain area, especially in the Greater and Lesser Hinggan Mountains areas in winter, which is significantly lower than that in the Songnen and Sanjiang Plains. The lower albedo in the Liaohe Plain in spring and winter is mainly attributed to the low snow cover caused by the southerly latitude because relative to the snow and ice underlying surface, the surface albedo in the Liaohe Plain is significantly lower than that in the Songnen and Sanjiang Plains. The surface albedo of a snow-free surface is relatively low. The underlying surface properties are the main factors affecting the levels of land surface albedo. The underlying surface properties in the Greater and Lesser Hinggan Mountains are mainly forest, whereas the underlying surface types in the Songnen and Sanjiang Plains are mostly cropland. We conclude that different land cover types have clear effects on land surface albedo, especially the differences between forest and cropland in winter. From the perspective of the spatial variation trend of surface albedo in different time periods in Northeast China, the surface albedo in the Greater and Lesser Hinggan Mountains showed a significant decrease trend in winter, which was largely related to the change in the degree of snow cover. After spring, the surface albedo increased significantly in the Songnen, Sanjiang, and northern Liaohe Plains. This may be related to the change in vegetation phenology caused by the change in land cover type.

4.4 Differences in surface albedo in different land cover types

To select the typical land cover types in the study area for analysis, we calculated the area and percentage of various land cover types in Northeast China in 2020. As shown in Table 2, although there are various types of land cover in Northeast China, including forest land, cropland, grassland, marsh, bare land, and water area, cropland and forest land are the two main types of land use in Northeast China, accounting for 88.42% of the total area of Northeast China, of which cropland area is the largest, followed by forest land. They account for 47.23 and 41.18% of the total area of Northeast China, followed by grassland, which accounts for 3.15%, and mosaic vegetation and urban areas, which account for 2.31 and 2.29% of the total study area, respectively. Specifically, the rainfed cropland is the main part of the cropland in Northeast China, accounting for 82.98% of the total cropland area, and the irrigated cropland is about 13.03%. The mixed cropland area is the smallest, accounting for only 1.88% of the total area in Northeast China. On the other hand, the forest land in Northeast China is mainly dominated by deciduous broadleaved forest and deciduous needleleaved forest, which account for more than

Table 2
Types of land cover in Northeast China and their areas and percentages.

Land cover abbreviation	Land cover type	Number of cells	Area ($\times 10^5$ km^2)	Percentage (%)
Rc	Rainfed cropland	4641107	3.13	39.19
Ic	Irrigated cropland	729047	0.49	6.16
Mc	Mosaic cropland	222919	0.15	1.88
Mv	Mosaic vegetation	273293	0.18	2.31
Ebf	Evergreen broadleaved forest	3643	0.00	0.03
Dbf	Deciduous broadleaved forest	3771707	2.54	31.85
Enf	Evergreen needleleaved forest	23236	0.02	0.20
Dnf	Deciduous needleleaved forest	928234	0.63	7.84
Mf	Mixed forest	150008	0.10	1.27
Mh	Mosaic herbaceous	38150	0.03	0.32
Sb	Shrubland	15945	0.01	0.13
Gl	Grassland	372962	0.25	3.15
Sv	Sparse vegetation	40302	0.03	0.34
Sw	Swamp	124596	0.08	1.05
Ua	Urban areas	270825	0.18	2.29
Ba	Bare areas	52105	0.04	0.44
Wb	Water bodies	183376	0.12	1.55

95% of the forest land area in Northeast China, 77.34 and 19.03%, respectively. From the perspective of spatial distribution, cropland is mostly distributed in the Songnen, Sanjiang, and Liaohe Plains, while forest land is mostly distributed in the Greater Khingan Mountains in the northwest, the Lesser Khingan Mountains in the north, and the Changbai Mountains in the southeast (Fig. 10).

In summary, land cover types with an area percentage greater than 2% were selected as typical land cover types in this study, which mainly included deciduous broadleaved forest, deciduous needleleaved forest, rainfed cropland, irrigated cropland, grassland, mosaic vegetation, and urban land cover types, accounting for 92.79% of the total area of Northeast China (Table 2).

In this study, the land surface albedo data for 20 years from 2001 to 2020 were used to analyze the seasonal changes in land surface albedo over different land cover types. Owing to the impact of human activities and climate change, land cover in Northeast China has undergone certain changes over the past 20 years. In an effort to eliminate the effect of land cover change on surface albedo, a total of 20 periods of CCI-LC land cover type data spanning from 2001 to 2020 were utilized in the present study. The average land surface albedo of different land cover types in Northeast China from 2001 to 2020 was extracted and analyzed annually to reveal the seasonal changes and differences in surface albedo of different land cover types in Northeast China.

Figure 11 shows the seasonal variations in land surface albedo on typical land cover types in spring, summer, autumn, and winter in Northeast China. The surface albedo values of the seven land cover types in Northeast China reach their maximum in winter, with the albedo values of all these land types exceeding 0.2. The albedo values of different land cover types, arranged from high to low, are rainfed cropland, irrigated cropland, grassland, mosaic vegetation, urban

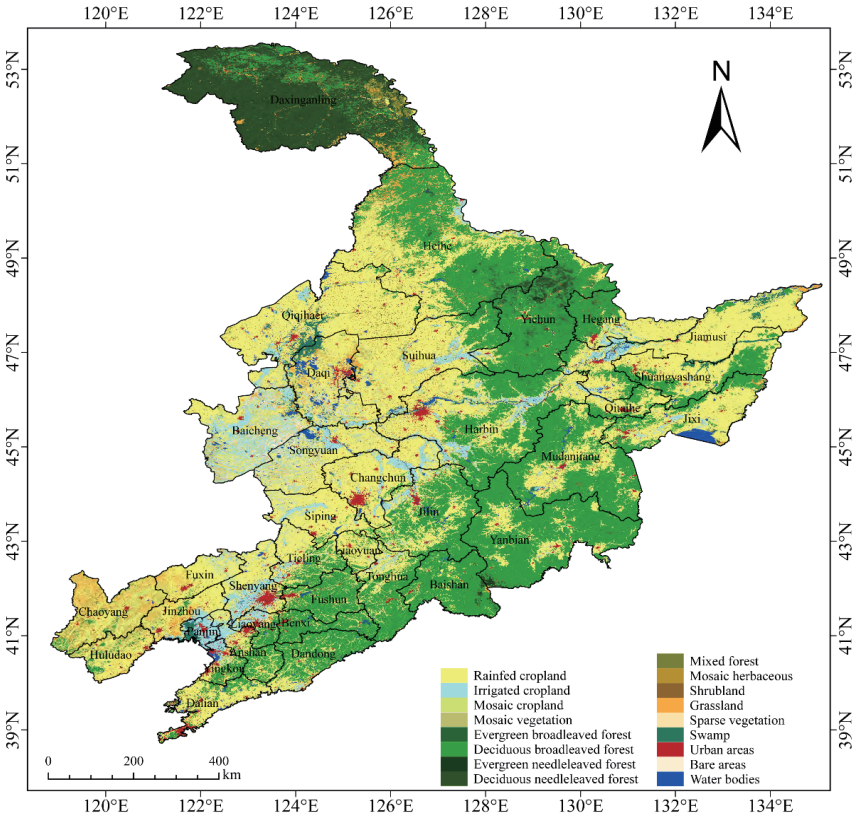

Fig. 10. (Color online) Spatial distribution of land cover in Northeast China in 2020.

areas, deciduous needleleaved forest, and deciduous broadleaved forest. Among them, the albedo value of rainfed cropland is approximately 0.463, which is nearly twice that of the deciduous broadleaved forest. The surface albedo reaches its minimum in summer, and the albedo values of different land cover types, arranged from high to low, are irrigated cropland, grassland, rainfed cropland, mosaic vegetation, urban areas, deciduous needleleaved forest, and deciduous broadleaved forest. However, the albedo values of these seven land types exhibit little variation, ranging from 0.12 to 0.15. The surface albedo values of different land cover types in spring and autumn are higher than the corresponding value in summer, and the surface albedo values range from 0.13 to 0.21. Note that in winter with snow, the surface albedo values of different land cover types are significantly higher than the albedo values in summer without snow. Owing to the significantly higher albedo values of snow than those of natural vegetation, in winter, the albedo values of sparse low-vegetation areas are higher, whereas those of dense high-vegetation areas are relatively low, primarily due to the shielding effect of the vegetation canopy. For instance, during winter, the albedo values of cropland exceed 0.41. In contrast, the albedo values of deciduous broadleaved forest and deciduous needleleaved forest remain relatively low, ranging only from 0.2 to 0.3. During summer, the surface albedo values of different land cover types in Northeast China show little disparity, where the difference between the irrigated cropland having the highest albedo values and the deciduous broadleaved forest with the lowest albedo

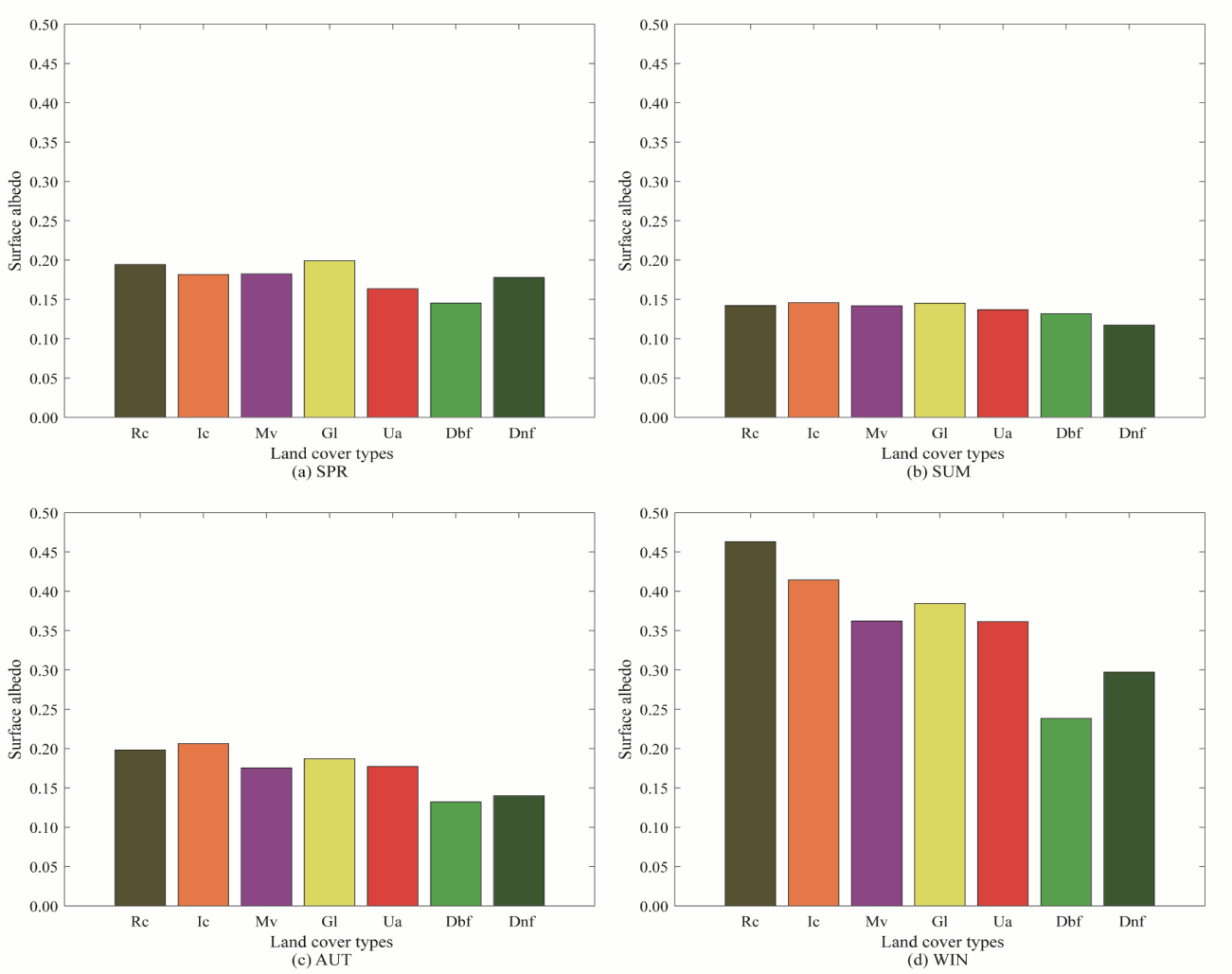

Fig. 11. (Color online) Surface albedo seasonal variations of different land cover types. (The abbreviations of land cover types in the figure follow those given in Table 3.)

values is lower than 0.03. According to the previous analysis, different land types exhibit pronounced seasonal fluctuations in surface albedo values.

In this study, we selected winter and summer to analyze the difference in surface albedo between of different land cover types in Northeast China. The results show (Table 3) that the albedo values of rainfed cropland in winter are the highest and are extremely significant compared with those of the other land types. The albedo values of irrigated cropland and grassland are second, with no significant difference between them. In winter, the albedo values of grassland, urban areas, and mosaic vegetation exhibit no significant difference. However, significant differences exist between these three land types and the other two, deciduous needleleaved forest and deciduous broadleaved forest. In summer, irrigated cropland exhibits the highest albedo, which shows extremely significant differences from that of all land types except grassland. Rainfed cropland shows extremely significant differences from all land types except

Table 3
Variance analysis results of surface albedo for different land cover types in winter and summer.

	Land cover type	Mean value	Significance	
			0.05	0.01
Winter	Rainfed cropland	0.463	a	A
	Irrigated cropland	0.414	b	B
	Grassland	0.385	b c	B C
	Mosaic vegetation	0.362	c	C
	Urban area	0.362	c	C
	Deciduous needleleaved forest	0.297	d	D
	Deciduous broadleaved forest	0.238	e	E
Summer	Irrigated cropland	0.146	a	A
	Grassland	0.145	a	A
	Rainfed cropland	0.142	b	B
	Mosaic vegetation	0.142	b	B
	Urban area	0.137	c	C
	Deciduous broadleaved forest	0.132	d	D
	Deciduous needleleaved forest	0.117	e	E

mosaic vegetation. Moreover, urban areas also have extremely significant differences from other land types. Furthermore, significant differences exist between deciduous needleleaved forest and deciduous broadleaved forest in summer. The data reveal that the surface albedo values vary significantly between different land cover types, especially in winter, which may be related to snow cover.

We quantitatively analyzed the surface albedo values of different land cover types under snow and nonsnow conditions. On the basis of MCD43A3 surface albedo data (average calculated every eight days) and MOD10A2 snow cover data from 2001 to 2020, we extracted the average surface albedo of seven land cover types under different conditions (with and without snow) and calculated their standard deviation. The albedo under snow conditions was extracted from the winter period (December to February of the following year), and the albedo under nonsnow conditions was obtained from the summer (June to August).

As shown in Table 4, under nonsnow conditions, the albedo values of different land cover types, arranged from high to low, are irrigated cropland, grassland, rainfed cropland, mosaic vegetation, urban areas, deciduous broadleaved forest, and deciduous needleleaved forest. Among these, the albedo of irrigated cropland is the highest, about 0.146, and that of deciduous needleleaved forest is the lowest, 0.117. The albedo values of rainfed cropland and deciduous broadleaved forest are 0.142 and 0.132, respectively. The predominant land cover types in Northeast China are forest land and cropland. However, under snow conditions, the albedo values, arranged from high to low, of different land cover types are rainfed cropland, irrigated cropland, grassland, mosaic vegetation, urban areas, deciduous needleleaved forest, and deciduous broadleaved forest. The surface albedo of rainfed cropland reaches 0.587, which is four times that under nonsnow conditions. Deciduous needleleaved forest and deciduous broadleaved forest exhibit relatively low surface albedo values, which are only two to three

Table 4
Surface albedo values and standard deviations of different land cover types.

Land cover type	Albedo (no snow)	Standard deviation	Albedo (snow)	Standard deviation
Rainfed cropland	0.142	0.003	0.587	0.077
Irrigated cropland	0.146	0.003	0.543	0.092
Mosaic vegetation	0.142	0.002	0.429	0.052
Deciduous broadleaved forest	0.132	0.003	0.311	0.035
Deciduous needleleaved forest	0.117	0.003	0.324	0.035
Grassland	0.145	0.003	0.519	0.062
Urban areas	0.137	0.003	0.362	0.063

times that under nonsnow conditions. It can be seen that forest loss leads to a significant increase in surface albedo, an effect that is particularly pronounced under winter snow cover. For instance, when deciduous needleleaved forest transitions to rainfed cropland, the surface albedo in summer without snow cover increases from 0.117 to 0.142, showing an increase of 0.025. In winter, owing to the presence of snow, the surface albedo increases from 0.324 to 0.587, an increase of 0.263, which is 10.5 times the increase in summer. On the other hand, against the backdrop of global warming, changes in the degree of snow cover will also cause different land cover types to shift from snow to nonsnow, and the albedo will inevitably change. As an illustration, take rainfed cropland where the albedo would shift from 0.587 to 0.142, a change of 0.445, which is greater than the 0.263 difference in albedo caused by forest loss under snow conditions. For other land cover types, this change remains substantial. For instance, the albedo of deciduous needleleaved forest decreased from 0.324 to 0.117, representing a reduction of 0.207. Therefore, the effect of snow cover changes on the albedo of different land types is extremely significant.

5. Discussion and Conclusions

5.1 Discussion

MODIS is a key sensor on board the Terra and Aqua satellites for Earth observation, providing abundant information for land, ocean, and atmosphere studies on a global scale. In this study, we utilized the MCD43A3 surface albedo product and the MOD10A2 snow cover product, both derived from the MODIS sensor, as well as the CCI-LC products provided by ESA, to analyze the interannual and seasonal variation characteristics of surface albedo in Northeast China. We quantitatively analyzed the relationship between these changes and surface cover types, especially the differences in surface albedo among different land cover types under snow and nonsnow conditions.

Williams *et al.* suggested that vegetation cover significantly affects the level of surface albedo, and a decrease in vegetation coverage will cause an increase in surface albedo.[24]

Davidson and Wang also found that the mean albedos of cropland and grassland are higher than those of broadleaved, needleleaved, and mixed forests, and that the effects of snow on the surface albedo differ considerably among cover types.[25] Weber *et al.* considered that the effect of forestation on surface albedo was more pronounced at higher latitudes than in the tropics owing to the lower albedo of the forest and seasonal snow cover (which considerably increases albedo for periods of the year when snow can settle on nonforested land).[26] As revealed in this study, the surface albedo variation process between different land cover types confirms these scientific conclusions. There are significant differences in albedo between sparse low-vegetation areas and dense high-vegetation areas, and forest land area reduction will cause a significant increase in albedo, particularly in winter when there is snow. This increase is 10.5 times that in summer.

The relationship between albedo and land cover could be affected by uncertainty in the data from different sources. The satellite-based data tend to have higher uncertainty in the Northeast region of China than in other areas owing to the complex surface conditions. In addition, the snow on different types of vegetation has different light-absorbing impurities and physical properties (e.g., grain size and density),[27] which also brings uncertainty to the research results. The effects of the uncertainty are difficult to quantify as the ground-based observational data are far from being sufficient, and the understanding of surface albedo over the study area is just beginning. In the future, generating high-quality satellite remote sensing data with finer resolution and more abundant ground-based observation data will enable a more accurate quantification of the relationship between albedo and land cover, and thus assess the effects of albedo changes on energy budget and ecosystems in depth.

5.2 Conclusions

In this study, we first utilized MODIS surface albedo product data (MCD43A3) to establish a long-time series database of surface albedo in Northeast China from 2001 to 2020. On the basis of this sequence, the spatiotemporal variation characteristics of surface albedo in Northeast China from 2001 to 2020 were analyzed. The results show the following: (1) The average annual surface albedo in Northeast China over the past 20 years has been about 0.21. From a temporal perspective, there has been almost no change in surface albedo over the past two decades, but there is a significant seasonal characteristic, with the highest surface albedo in winter, averaging about 0.36, followed by spring and autumn, at 0.18 and 0.17, respectively, and the lowest in summer, at only 0.13. There are significant differences among surface albedo across different seasons; specifically, there is a highly significant difference between winter and summer ($P < 0.01$), and both winter and summer seasons show highly significant differences compared with spring and autumn ($P < 0.01$), whereas there is no significant difference in surface albedo between spring and autumn. (2) Spatially, the surface albedo in Northeast China from 2001 to 2020 exhibits distinct heterogeneity; it is generally characterized by higher values in the east and west, and lower values in the south, north, and central areas during winter, spring, and autumn.

In summer, the surface albedo exhibits uniformity across the entire study area, and the spatial heterogeneity is unclear. The spatial distribution characteristics of surface albedo are closely related to the land cover types in the study areas. The predominant land cover types in Northeast China are forests and cropland, collectively constituting approximately 88.42% of the total area of Northeast China. Forests are predominantly distributed in the northern, northwestern, and southeastern parts of the study area. In contrast, the eastern and western regions are the Sanjiang and Songnen Plains, respectively, where the land cover is mainly cropland. In terms of spatial variation, there is a significant decreasing trend in surface albedo in the northwestern Daxing'anling area during spring and winter. The regions with substantially increased surface albedo during summer and autumn are predominantly distributed in the southern part of the study area and the Songnen Plain, which is located in the west of the study area. (3) To explore the relationship between land cover and surface albedo, we statistically analyzed surface albedo on typical land cover types within the study area and found that the surface albedo varies significantly across different land cover types in each season, which is mainly manifested as the significant difference in albedo between sparse low-vegetation and dense high-vegetation areas. This difference is particularly pronounced in winter when there is snow, notably after forests give way to cropland, and the increase in albedo is 10.5 times that in summer.

Acknowledgments

This work was supported by the Fundamental Research Funds for the Central Universities of the Department of Education of Heilongjiang Province (Grant No. 2022-KYYWF-0592), the Natural Science Foundation of Heilongjiang Province (Grant No. PL2024C005), and the Doctoral Fund Project of Jiamusi University (Grant No. JMSUBZ22-03).

References

1 J. Chen, C. Lei, H. Chu, X. Li, M. Torn, Y.-P. Wang, P. Sciusco, and G. P. Robertson: Environ. Res. Lett. **19** (2024) 093001. https://doi.org/10.1088/1748-9326/ad661d
2 C. A. Gueymard, V. Lara-Fanego, M. Sengupta, and Y. Xie: Sol. Energy. **182** (2019) 194. https://doi.org/10.1016/j.solener.2019.02.040
3 J. G. Charney: Q. J. R. Meteorolog. Soc. **101** (1975) 193. https://doi.org/10.1002/qj.49710142802
4 N. Zeng and J. Yoon: Geophys. Res. Lett. **36** (2009). https://doi.org/10.1029/2009GL039699
5 J. Chen: Acta Geogr. Sin. **31** (1964) 85 (in Chinese). https://doi.org/10.11821/xb196402001
6 S. Liu, S. Li, G. Yu, X. Sun, L. Zhang, M. Sugita, Y. Li, X. Zhang, and Y. Wang: Acta Ecol. Sin. **30** (2010) 557 (in Chinese). www.ecologica.cn/stxb/article/abstract/stxb200811070330
7 G. Zhang, G. Zhou, and F. Yang: Acta Ecol. Sin. **30** (2010) 6943 (in Chinese). www.ecologica.cn/stxb/article/abstract/stxb200911141507
8 S. Wang, Y. Hu, S. Wang, K. Shang, and D. Yan: Remote Sens. Technol. Appl. **30** (2015) 932 (in Chinese). http://www.rsta.ac.cn/CN/10.11873/j.issn.1004-0323.2015.5.0932
9 T. d. O. Faria, T. R. Rodrigues, L. F. A. Curado, D. C. Gaio, and J. S. Nogueira: Rev. Ambient. Água **13** (2018) e2120. https://doi.org/10.4136/ambi-agua.2120
10 X. Zhang: Geogr. Res. **31** (2012) 299 (in Chinese). https://www.dlyj.ac.cn/CN/10.11821/yj2012020010
11 Z. Xu, X. Qiu, S. Li, G. Shi, and Y. He: J. Arid Land Resour. Environ. **34** (2020) 99 (in Chinese). https://doi.org/10.13448/j.cnki.jalre.2020.014

12 K. Atlaskina, F. Berninger, and G. de Leeuw: TC. **9** (2015) 1879. https://doi.org/10.5194/tc-9-1879-2015
13 G. Pang, D. Chen, X. Wang, and H.-W. Lai: Sci. Total Environ. **804** (2022) 150100. https://doi.org/10.1016/j.scitotenv.2021.150100
14 Y. Ding and X. Dai: Meteor. Mon. **20** (1994) 19 (in Chinese). http://qxqk.nmc.cn/qx/ch/reader/view_abstract.aspx?file_no=19941208&st=alljournals
15 J. Zhang, S. Chen, and X. Zhao: J. Arid Land Resour. Environ. **20** (2006) 1 (in Chinese). https://doi.org/10.3969/j.issn.1003-7578.2006.04.001
16 S. Liang, H. Fang, M. Chen, C. J. Shuey, C. Walthall, C. Daughtry, J. Morisette, C. Schaaf, and A. Strahler: Remote Sens. Environ. **83** (2002) 149. https://doi.org/10.1016/S0034-4257(02)00092-5
17 N. Kuusinen, E. Tomppo, Y. Shuai, and F. Berninger: Remote Sens. Environ. **145** (2014) 145. https://doi.org/10.1016/j.rse.2014.02.005
18 M. A. Faiz, D. Liu, A. A. Tahir, H. Li, Q. Fu, M. Adnan, L. Zhang, and F. Naz: Atmos. Res. **231** (2020) 104653. https://doi.org/10.1016/j.atmosres.2019.104653
19 Q. Liu, Y. Zhang, L. Liu, L. Li, and W. Qi: Geogr. Res. **36** (2017) 2061 (in Chinese). https://www.geores.com.cn/EN/abstract/abstract39798.shtml
20 Y. Yang, P. Xiao, X. Feng, and H. Li: ISPRS J. Photogramm. Remote Sens. **125** (2017) 156. https://doi.org/10.1016/j.isprsjprs.2017.01.016
21 D. Liu, L. Zhang, S. Jiang, S. Shi, and Y. Li: Phys. Chem. Earth. A/B/C. **116** (2020) 102832. https://doi.org/10.1016/j.pce.2019.102832
22 T. Pan, L. Zhang, H. Zhang, C. Ren, and Y. Li: Phys. Chem. Earth. A/B/C. **115** (2020) 102828. https://doi.org/10.1016/j.pce.2019.102828
23 S. Das and S. Banerjee: Arabian J. Geosci. **14** (2021) 946. https://doi.org/10.1007/s12517-021-07313-x
24 C. A. Williams, H. Gu, and T. Jiao: Sci. Adv. **7** (2021) eaax8859. https://doi.org/10.1126/sciadv.aax8859
25 A. Davidson and S. Wang: Can. J. Remote Sens. **31** (2005) 377. https://doi.org/10.5589/m05-021
26 J. Weber, J. A. King, N. L. Abraham, D. P. Grosvenor, C. J. Smith, Y. M. Shin, P. Lawrence, S. Roe, D. J. Beerling, and M. V. Martin: Sci. **383** (2024) 860. https://doi.org/10.1126/science.adg6196
27 R. Garzonio, B. Di Mauro, S. Cogliati, M. Rossini, C. Panigada, B. Delmonte, V. Maggi, and R. Colombo: Cold Reg. Sci. Technol. **155** (2018) 47. https://doi.org/10.1016/j.coldregions.2018.07.005

About the Authors

Tao Pan received his B.S., M.S., and Ph.D. degrees from Harbin Normal University, China, in 2014, 2017, and 2022, respectively. Since 2022, he has been a lecturer at Jiamusi University, China. His research interests are in geographic information system and remote sensing. (pantao@jmsu.edu.cn)

Fu Li received his B.S., M.S., and Ph.D. degrees from Harbin Normal University, China, in 2003, 2007, and 2019, respectively. Since 2020, he has been an associate professor at Jiamusi University, China. His research interests are in environmental ecological effects and resource utilization. (lifu@jmsu.edu.cn)

Yu Cheng Tao received his B.S. degree from Jilin International Studies University, China, in 2021 and his M.S degree from Jiamusi University, China, in 2025. His research interests are in remote sensing and geographic information system applications. (1026749547@qq.com)

Li Juan Zhang received her B.S. degree from Nanjing University of Information Science and Technology, China in 1983 and her Ph.D. degree from Nanjing Agricultural University, China, in 2006. Since 2007, she has been a professor at Harbin Normal University. Her research interests are in cryosphere remote sensing. (zhlj@hrbnu.edu.cn)

Xiaoyan Jiang received her B.S. and M.S. degrees from Harbin Normal University, China, in 2017 and 2022, respectively. Since 2024, she has been a lecturer at Jiamusi University, China. Her research interests are in satellite data analysis and applications.
(jiangxiaoyan@jmsu.edu.cn)